Microchimica Acta (2022) 189:412
https://doi.org/10.1007/s00604-022-05485-1

ORIGINAL PAPER

Design and fabrication of a sensitive electrochemical sensor for uranyl ion monitoring in natural waters based on poly (brilliant cresyl blue)

Zhiping Zhou[1,2] · Yueming Zhou[2] · Xizhen Liang[2] · Jianqiang Luo[2] · Shujuan Liu[2] · Jianguo Ma[2]

Received: 21 May 2022 / Accepted: 29 August 2022 / Published online: 10 October 2022

Abstract

New insights are proposed into enhancing detection of uranyl ions (UO_2^{2+}) by electropolymerization brilliant cresyl blue–modified glassy carbon electrode (PBCB/GCE). The mercury-free PBCB/GCE sensor was applied to determine UO_2^{2+} in water samples by differential pulse adsorptive stripping voltammetry (DPAdSV). The unique combination of the PBCB/GCE and DPAdSV significantly improves sensitivity due to the polymer of high electroactive area and fast electron transfer rate. The DPAdSV current using a 3 mm diameter PBCB/GCE was proportional to the UO_2^{2+} concentration in the range 2.0–90.0 μg·L^{-1} (− 0.113 V vs. SCE) with a detection limit of 0.650 μg·L^{-1}, RSD = 3.1% (n = 10), and 4.5% reproducibility. In addition, the sensitivity for UO_2^{2+} determination was further improved at using an 1 mm diameter PBCB/GCE, which enhances the efficiency of UO_2^{2+} deposition due to its higher current density. The 1 mm diameter PBCB/GCE based on DPAdSV technique could be used to determine uranyl ions in the concentration range 0.20–2.0 μg·L^{-1} (− 0.113 V vs. SCE) with a detection limit of 0.067 μg·L^{-1}, RSD = 5.7 % (n = 10) and 5.4% reproducibility. Hence, the PBCB/GCE is a suitable candidate to substitute the mercury electrode.

Keywords Uranyl ions · Brilliant cresyl blue · Electropolymerization · Differential pulse adsorptive stripping voltammetry

Introduction

Uranium and its compounds are called the new energy elite because they are widely used in nuclear power and nuclear military industry [1–4]. However, their development, production, and usage may generate lots of radioactive waste into the environment, which poses a serious hazard to humans, like immune system damage, cancer, and birth defects [5–7]. In addition, unlike most metal ions, uranium has many valences in aqueous solutions, and uranyl ions (UO_2^{2+}) are the predominant ionic species in aqueous solution [2, 8]. A simple, fast, and in situ UO_2^{2+} detection method will help with process monitoring, environmental remediation, and minimization of UO_2^{2+} exposure to humans [9]. Due to the low concentration of UO_2^{2+} in the natural environment and the complexity of the sample matrix, these factors seriously interfere with the quantitative detection of UO_2^{2+}.

In recent years, significant progress has been made in UO_2^{2+} monitor using a selection of physical techniques and chemical sensors [10–21]. Several conventional techniques for analyzing UO_2^{2+}, such as inductively coupled plasma-optical emission spectroscopy (ICP-OES) [22, 23], inductively coupled plasma-mass spectroscopy (ICP-MS) [24], spectroscopy methods [21, 25] and neutron activation analysis [26, 27], require professional operators, complex apparatuses, and high maintenance costs. Nowadays, portable sensors for uranium detection have been developed. For example, Chen et al. [10] used gold nanoparticles and hybridization chain reaction–assisted synthesis of silver nanoclusters for electrochemical sensing for the sensitive detection of uranyl ions. A.R. Salem et al. [13] reported a cyanopyridine-derived fluorescent sensor for the selective determination of uranyl ions in different water samples. W. He and D. Hua employed

✉ Yueming Zhou
ymzh@iccas.ac.cn

✉ Jianguo Ma
mjgyh8125@163.com

[1] Sino-French Institute of Nuclear Engineering and Technology, Sun Yat-sen University, Zhuhai, Guangdong 519082, People's Republic of China

[2] State Key Laboratory of Nuclear Resources and Environment, East China University of Technology, Nanchang 330013, People's Republic of China

spectrographic sensors for uranyl detection in the environment. In contrast, electrochemical is a simple, fast, low-cost, superior spatial and temporal resolution for in situ monitoring technology of UO_2^{2+} [28, 29]. In addition, UO_2^{2+} detection by electrochemical methods has also played an indispensable role in the design of uranyl sensors [28, 29]. Adsorption stripping voltammetry (AdSV) based on mercury electrodes can accurately measure heavy metal ions and detect uranyl ions by combining with a complexing agent [30–32]. Sensitive detection of UO_2^{2+} in the presence of cupferron has been studied [3, 4, 16, 33–36]. For example, Zhang L et al. [3] proved that the diphenylguanidine radical cations induce adsorption of $[^{VI}UO_2^{2+} - Cupferron]$ during preconcentration, resulting in higher response currents.

Chemically modified electrodes (CMEs) made of conducting polymers (CPs) have attracted extensive interest in the fields of electrochemistry and electroanalysis due to their higher electroactive surface area, excellent conductivity, and electrocatalytic effects [36–41]. CPs deposited on the surface of electrodes, like poly Nile blue (PNB) [16], poly neutral red (PNR) [40], and poly(3,4-ethylenedioxythiophene) (PEDOT) [42], were used to detect heavy metal ions. Among different CPs used, poly brilliant cresyl blue (PBCB) emerges as an efficient electrode material with properties for bioanalytical science due to its rigid planar structures, redox, and simple electropolymerization processes [36, 37, 39, 43, 44]. In previous work [43, 44], we investigated electropolymerization of PBCB and NR on carbon-nanotube–modified electrodes in binary and ternary deep eutectic solvents, as well as the determination of epinephrine using graphene/PBCB/GCE. Because UO_2^{2+} has a linear structure with two nonreactive double uranium-oxygen bonds [45, 46], the most sensitive electrodes detected UO_2^{2+} using complexing reagents [47]. At present, there are no reports on the application of PBCB/GCE as an electrochemical sensor for UO_2^{2+}. Therefore, exploring the determination of UO_2^{2+} is interesting and challenging on PBCB/GCE.

In this work, we developed a new strategy to enhance the sensitive detection of UO_2^{2+} by differential pulse adsorption stripping voltammetry (DPAdSV) on PBCB/GCE. The effects of several parameters were investigated, like electropolymerization potential, electropolymerization cycles, BCB monomer concentration, pH values, concentration of complexing agent, deposition potential, and deposition time. Compared to previous work [4], the PBCB/GCE significantly improves the sensitivity of UO_2^{2+} detection and reaches a lower level of sub-part-per-billion, which was attributed to the PBCB polymer of high conductivity, larger electroactive area, and redox activity. Therefore, the DPAdSV based on PBCB/GCE was applied for the determination of UO_2^{2+} in real water samples.

Experimental section

Instrumentation

The cyclic voltammetry (CV), electrochemical impedance spectroscopy (EIS), and DPAdSV measurements were performed using PARSTAT 2273 (AMET Co., Ltd., Princeton, USA). A three-electrode cell with a volume of 25.0 mL was used. As a working electrode, modified electrodes (PBCB/GCE) with diameters of 1 or 3 mm were used.

The modified electrode was made in the following manner: the GCE polishing and cleaning was described in Ref. [4, 16]. After the treatment of GCE, it was immersed in a freshly prepared solution containing 0.50 mM of brilliant cresyl blue (BCB) in 0.10 M pH 6.80 Na_2HPO_4/NaH_2PO_4 containing 0.20 M $NaNO_3$, to obtain PBCB/GCE by CV electrochemical polymerization. The fabrication of PBCB/GCE was described in Ref. [43], and then, PBCB/GCE was put in a CH_3COOH/CH_3COONa (pH 5.00) solution for further study after being washed with sub-boiling double-distilled water (DDW). A schematic diagram of the PBCB/GCE in Scheme 1 as well as its real electrochemical polymerization process is presented in Fig. S1a-b, respectively. The EIS measurements were carried out at a frequency range from 1.0×10^5 to 1.0×10^{-2} Hz and with a 5-mV amplitude of the AC signal. Platinum foil and a saturated calomel electrode (SCE) filled with saturated KCl were used as the auxiliary and reference electrodes, respectively. The morphology of the modified electrodes was observed using NNS450 scanning electron microscopy (SEM) (FEI Czech Co., Ltd., Czech). The pH measurements were performed with a ST-2100 pH meter (Ohaus International Trade Co., Ltd., China).

Reagents

All chemicals, namely, cupferron (≥ 98% purity, Aladdin), diphenylguanidine (DPhG) (≥ 97% purity, Aladdin), CH_3COOH/CH_3COONa (≥ 99% purity, Aladdin), NaOH (≥ 99% purity, Sinopharm), nitric acid (≥ 99% purity, Sinopharm), and Na_2HPO_4/NaH_2PO_4 (≥ 99% purity, Sinopharm) were used as received. $UO_2(NO_3)_2{\cdot}6H_2O$ stock solution was prepared by dissolving U_3O_8 powders (≥ 99% purity, China National Nuclear Corporation) in 6.0 M diluted nitric acid. A fresh solution of 0.020 M cupferron was obtained in sub-boiling DDW. DPhG (0.020 M) was prepared by diluting the appropriate amount of reagent in ethanol. CH_3COOH/CH_3COONa (0.10 M) was prepared under different conditions by mixing the stock solution of CH_3COOH and CH_3COONa. Na_2HPO_4/NaH_2PO_4 (0.10 M) was prepared under different conditions by mixing the

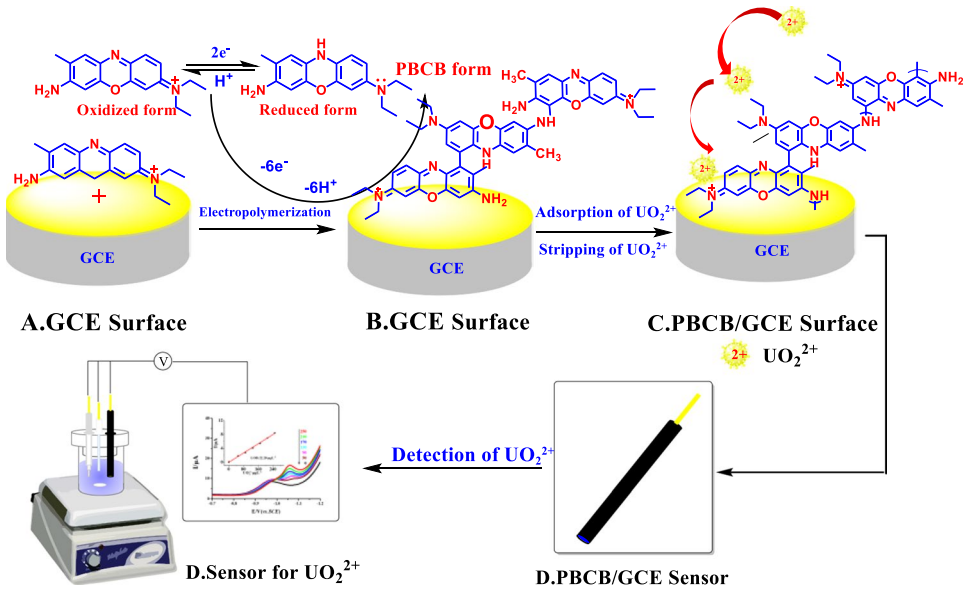

Scheme 1 A schematic illustration of the preparation of PBCB/GCE.

stock solution of NaH_2PO_4 and Na_2HPO_4. NaOH (2.0 M) used in pH optimization studies was prepared by dilution of 30% reagent.

Analytical procedure

The detection of UO_2^{2+} was performed in an electrochemical cell containing 0.10 M CH_3COOH/CH_3COONa (pH 5.00) and a certain concentration of cupferron and diphenylguanidine. The deposition of UO_2^{2+} was carried out at − 0.95 V (*vs.* SCE) under stirring with a deposition time of 180 s, and then the differential pulse voltammetry (DPV) stripping was recorded in quiescent solution from 0.30 to − 1.20 V (*vs.* SCE) by DPAdSV. The measuring cell was also equipped with a PTFE stirrer, which was used for stirring the solutions during the deposition process at a speed of 750 rpm. The stirring rate, scan rate, pulse height, step height, step time, deposition potential, and deposition time were 750 rpm, 8 $mV{\cdot}s^{-1}$, 50 mV, 4 mV, 0.5 s, − 0.95 V, and 180 s, respectively. The PBCB/GCE for DPAdSV measurement was obtained after electrochemically cleaning, which includes 1–4 DPVs. Each measurement was repeated thrice. All electrochemical experiments were carried out without solution deoxygenation at room temperature.

Real samples preparation

Three real samples (Tap Water from our laboratory, Bohai Sea Water in the city of Weihai, Shandong, China, and Yangtze River Water in the City of Nanjing, Jiangsu, China) were prepared to evaluate the performance of the electrode. The water samples were simply filtered with a long-neck funnel to remove insoluble substances, and then the sample acidified before being sealed for refrigeration. A 5.00 mL water sample was fractioned in 25.0 mL volumetric flask containing 0.10 M CH_3COOH/CH_3COONa pH 5.00, 200 µM cupferron, and 80.0 µM diphenylguanidine, and then detected using DPAdSV.

Results and discussion

Characterization of PBCB/GCE

The EIS techniques provide an excellent method to examine the interfacial impedance of the electrode/film/solution interface [43, 48]. EIS measurements were carried out to examine the electron transfer resistance (R_{ct}) and bode plots of PBCB/GCE and GCE shown in Fig. 1a and Fig. S2, respectively. Obviously, the R_{ct} of PBCB/GCE was smaller than bare GCE, which was attributed to the faster charge transfer kinetics at PBCB/GCE in Table S1. Besides, the bode angle of PBCB/GCE was larger than bare GCE, indicating the higher electrochemical activity at PBCB/GCE. As shown in Fig. 1b, the electrochemical features of PBCB/GCE and GCE by CV were investigated using 10.0 mM $K_3[Fe(CN)_6]$ containing 0.10 M KCl as the redox probe [48]. A higher peak current (curve a) was observed on PBCB/GCE, implying that PBCB/GCE could accelerate electron transfer. In addition, the PBCB/GCE (curve a) obtained a smaller peak potential difference (ΔE_p) of anodic and cathodic than bare GCE (curve b), which suggests that the positive charged PBCB with good conductivity was favorable for the approach of $Fe(CN)_6^{3-/4-}$.

SEM analysis of the electrodes provides more information about the GCE and PBCB/GCE shown in Fig. 1c,

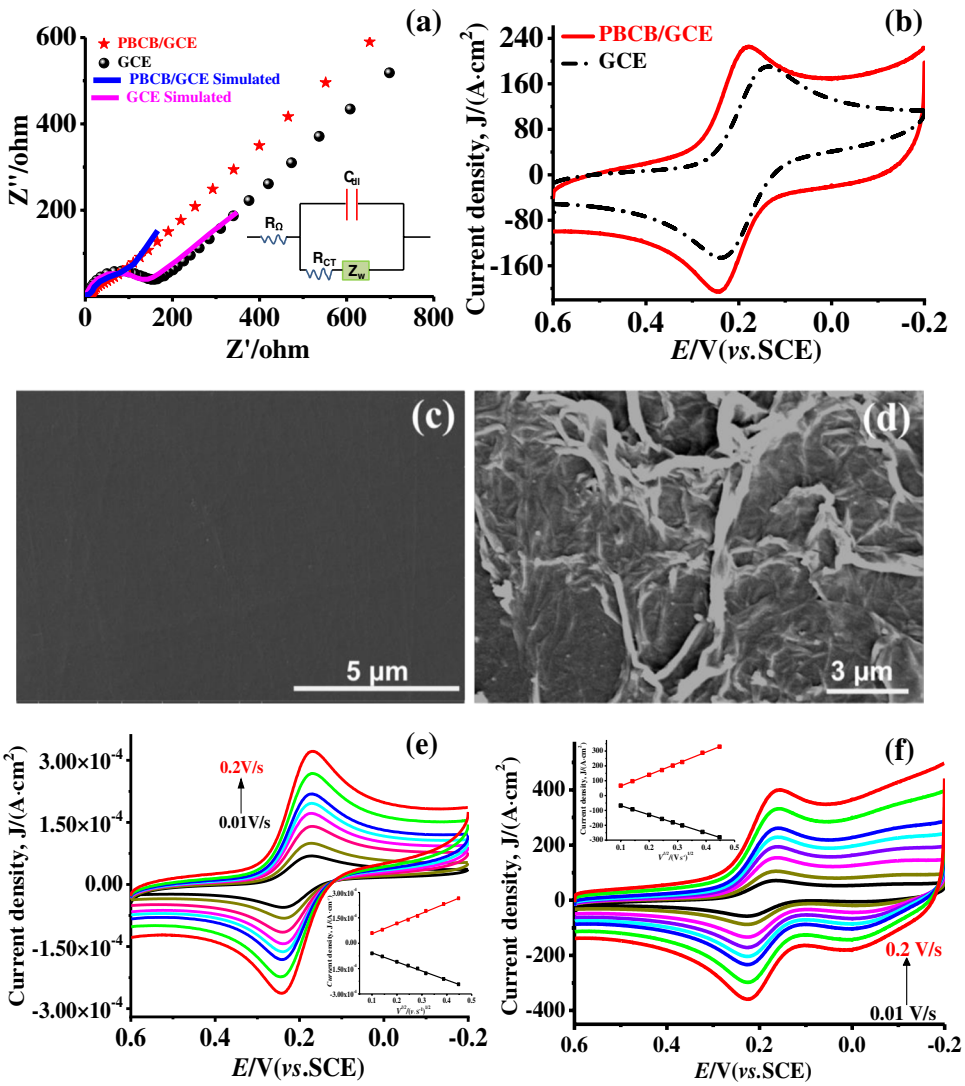

Fig. 1 **a** EIS and **b** CV of PBCB/GC and GCE in the solution containing 10.0 mM K_3[Fe $(CN)_6$] and 0.10 M KCl. Z′ and Z″ are the real and imaginary components, respectively. Inset is the circuit model for the modified electrodes. SEM images of the vertical-section of a fold-thrust belt 3D structure **c** GCE and **d** PBCB/GCE. Cyclic voltammograms of *Φ* 3 mm (**e**) GCE and (**f**) PBCB/GCE at different scan rates in the solution containing 1.0 mM K_3[Fe $(CN)_6$] and 0.20 M KNO_3. Inset shows the variation of peak current with square root of scan rate

d, respectively. The vertical-section view allows confirming the fold-thrust belt structure, which increases the electroactive area. In addition, the highly porous structure of poly (brilliant cresol blue) seems to promote the deposition of analytes on the surface, suggesting that PBCB/GCE increases the electroactive area as compared with GCE. As shown in Fig. 1e, f, the electrochemically active surface area (EASA) of electrodes by cyclic voltammetry was measured. According to the *Randles-Sevcik* equation [49], the EASA of GCE and PBCB/GCE were calculated to be 0.016 and 0.022 cm^2, respectively. Therefore, excellent conductivity and high electroactive area may be favorable to the adsorption and stripping process of uranium on the surface of PBCB/GCE.

The performance of the PBCB/GCE determination of UO_2^{2+}

With non-toxic materials, CP-modified electrodes improve sensitivity compared with glassy carbon electrodes due to their unique properties [36, 41]. Besides, the eco-friendly character of the proposed PBCB/GCE originates from the amount of non-toxic.

Figure 2 a and Fig. S3 show stripping voltammograms at the PBCB/GCE for 20.0 μg·L^{-1} UO_2^{2+} in the presence of cupferron and diphenylguanidine. It can be seen in Fig. 2a that a higher cathode peak (·) was exhibited at − 1.13 V (*vs.* SCE) with a current density (J_p) of approximately 205 μA·cm^{-1}, which was in accordance with previous published work [3]. Besides, the cathodic peak was obtained for the reduction of $^{VI}UO_2^{2+} - Cupferron$ to $^{III}U^{3+} - Cupferron$ at − 1.13 V (*vs.* SCE), which was very similar to the result of Paneli M et al. [50]. Meanwhile, no peak was observed for the reduction of $^{VI}UO_2^{2+} - Cupferron$ to $^{III}U^{3+} - Cupferron$ at − 0.30 V (*vs.* SCE), which was masked by the larger reduction wave of oxygen. As shown in the inset Fig. 2a, adequate information on the peak of analysis for UO_2^{2+} was provided in the potential range, which was supported by previous studies [3, 16, 33, 34].

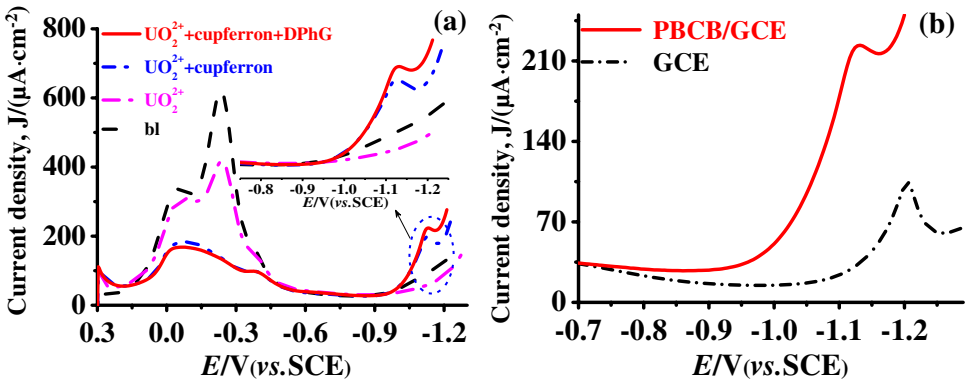

Fig. 2 DPAdSV in 0.10 M CH_3COOH/CH_3COONa of pH 5.00 for a 20.0 μg·L^{-1} UO_2^{2+} with 200 μM cupferron and 80.0 μM diphenylguanidine (·), 20.0 μg·L^{-1} UO_2^{2+} with 200 μM cupferron (:), 20.0 μg·L^{-1} UO_2^{2+} (·) and blank solution (·) at PBCB/GCE, **b** Stripping response at PBCB/GCE (·) and GCE (·) in 20.0 μg·L^{-1} UO_2^{2+} with 200 μM cupferron and 80.0 μM diphenylguanidine

Figure 2b compares the adsorptive stripping voltammetry responses obtained for UO_2^{2+} at the PBCB/GCE and GCE. Compared to GCE, the PBCB/GCE obtained a higher stripping peak current due to electrocatalytic effects or high electroactive area. Besides, the reduction peak potential of UO_2^{2+} (·) shifted to a relatively positive potential, which suggests that the polymer of PBCB may accelerate the uranium-cupferron electron transfer, leading to easier reduction of UO_2^{2+}. On the other hand, the E_p of 20.0 μg·L^{-1} UO_2^{2+} toward the relatively positive potential shifted 160 mV, and the J_p of 20.0 μg·L^{-1} UO_2^{2+} increased 2.5 times compared to those with bare GCE. These results confirm that the sensitivity improvement is related to the highly active area and excellent conductivity of the PBCB polymer.

Effect of the potential window, the concentration of BCB monomer, and electropolymerization cycles on the properties of the PBCB/GCE

Because the PBCB polymer of electropolymerization involves several steps, including radical-cation generation, oligomer formation, nucleation, and polymer growth [39, 51]. In order to study the effect of the CV electropolymerization, potential window on the performance of PBCB/GCE was utilized. The electropolymerization process was induced at different initial potential windows such as 0.20–1.2 V, 0.40–1.4 V, 0.60–1.8 V, and 0.80–1.8 V (*vs.* SCE); then, the electropolymerization potential window was switched to − 0.80 to 1.8 V (vs .SCE) for 15 CVs, and finally, different PBCB/GCE electrodes were obtained. As shown in Fig. 3a, the electrochemical properties of these polymer films were characterized by CV in 0.10 M pH 6.80 Na_2HPO_4/NaH_2PO_4 containing 0.20 M $NaNO_3$. The effect of the initiating electropolymerization potential window on the J_p of 20.0 μg·L^{-1} UO_2^{2+} is investigated in Fig. 3b. The increase of the J_p of UO_2^{2+} was severely affected by the initial potential of CV electropolymerization, such as 0.80–1.8V and 0.60–1.60V (*vs.* SCE). Due to the defects on electrode surface and crosslinked material formation, a higher oxidation potential was caused [39]. In addition, higher potentials will accelerate the oxygen bubbles generated by the electrolyzed water, which will affect the formation of the membrane and the service life of the electrode substrate; therefore, the initiation potential of 0.80–1.80V (*vs.* SCE) was selected for the following experiments.

The concentration of the BCB monomer was changed from 0.050 to 1.0 mM, and its influence on the J_p of 20.0 μg·L^{-1} UO_2^{2++} was studied. The obtained results are presented in Fig. 4a. It was observed that the J_p of UO_2^{2+} attained its maximum value at BCB monomer concentration of 0.50 mM. The number of voltammetry cycles was changed from 5 to 30 cycles and its effect on the J_p of 20.0 μg·L^{-1} UO_2^{2+} was investigated in Fig. 4b. It can be clearly seen that the J_p of 20.0 μg·L^{-1} UO_2^{2+} rapidly increases with

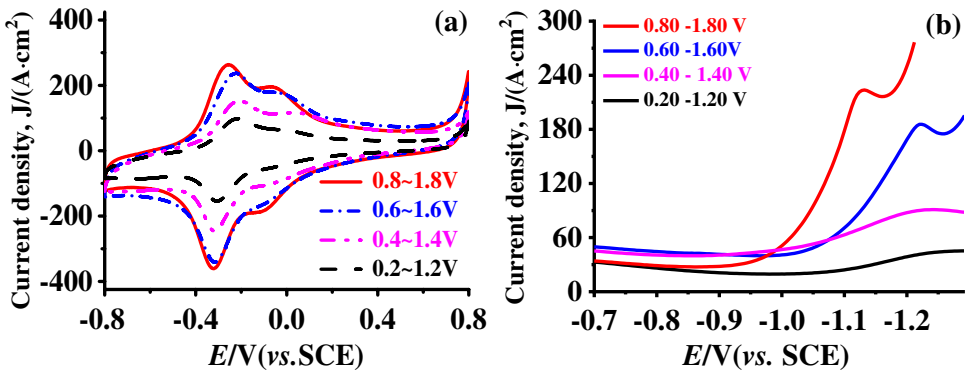

Fig. 3 **a** Effect of the electropolymerized potential, **b** effect of the different initiation potentials on the stripping response of 20.0 μg·L^{-1} UO_2^{2+} and blank

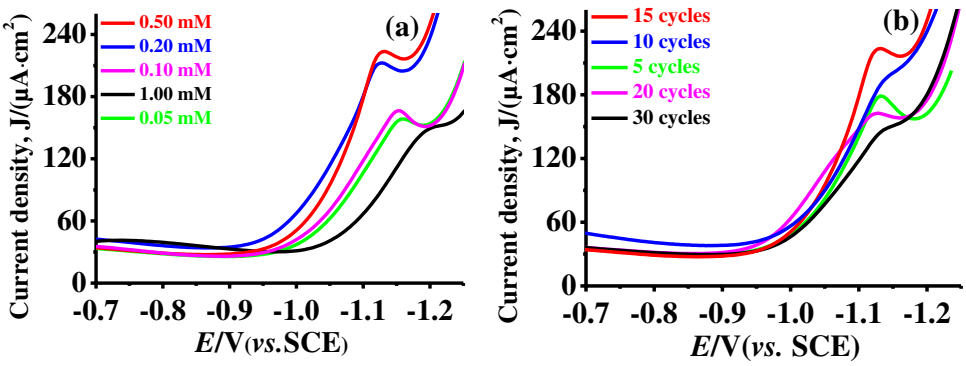

Fig. 4 DPAdSV in 0.10 M CH_3COOH/CH_3COONa of pH 5.00 for **a** effect of the concentration of BCB monomer and **b** the electropolymerization of cycles on the peak current of 20.0 μg·L^{-1} UO_2^{2+}

increasing the number of cycles from 5 to 15, and then the J_p of UO_2^{2+} decreased at more than 15 cycles. Therefore, the potential windows of 0.8–1.8 V (*vs.* SCE), BCB monomer concentration, and the number of voltammetry cycles was 0.50 mM and 15 cycles, respectively. These values were chosen for further investigations.

Effect of the uranium-cupferron reaction conditions

On the basis of previous literature studies, an acetate buffer was used as the main supporting electrolyte [30, 34]. The pH value of the CH_3COOH/CH_3COONa solution was changed from 3.00 to 6.00. The results obtained are shown in Fig. S4. On the basis of these results, the pH 5.00 was chosen for further study.

Since uranyl ions have a linear structure with two non-reactive uranium-oxygen bonds [2], complexing reagents are required for sensitive detection of UO_2^{2+} [30]. As shown in Fig. S5a-b, the concentration of the cupferron was changed from 40.0 to 560 μM and its effect on the net current density of cupferron and $[^{VI}UO_2^{2+} - Cupferron](\Delta J_p = J_{p(UO_2^{2+})} - J_{p(bl)})$ was studied. It was found that the current of the ΔJ_p of 20.0 and 5.00 μg·L^{-1} UO_2^{2+} increases as the concentration of cupferron increases to 200 μM and then slowly decreases. The concentration of cupferron 200 μM was chosen for further study. In addition, the concentration of diphenylguanidine was changed from 20.0 to 140 μM, and its effect on the ΔJ_p of 20.0 and 5.00 μg·L^{-1} UO_2^{2+} was investigated, as shown in Fig. S6. The ΔJ_p for UO_2^{2+} increases as diphenylguanidine concentration increases to 80.0 μM and then becomes nearly stable, so diphenylguanidine concentration of 80.0 μM was chosen for further study.

Effect of the stirring

In order to optimize the effect of stirring rate on 20.0 and 5.00 μg·L^{-1}, UO_2^{2+} J_p were investigated between 0 and 1000 rpm, whereas the other parameters were kept constant. As shown in Fig. S7, the uranium peak increased linearly with the stirring rate up to 500 rpm, then more slowly up to 750 rpm and leveled off, which indicated that $[^{VI}UO_2^{2+} - Cupferron]$ was strongly adsorptive on the surface of PBCB/GCE. The polymer of PBCB film may capture UO_2^{2+} via noncovalent interactions between the oxygen atoms of the UO_2^{2+} and the hydrogen atom of the amino group in deposition process. However, increasing the stirring rate had no effect on the stripping peak. Therefore, a stirring rate of 750 rpm was chosen as the optimal value for further experiments.

Effect of the deposition potential and time

The effect of the deposition potential was studied for UO_2^{2+} concentrations of 20.0 and 5.00 μg·L^{-1}, as shown in Fig. S8a. The potential was changed from − 0.70 to − 1.20 V (*vs.* SCE). It was observed that the J_p of UO_2^{2+} increases as the potential changes from − 0.70 to − 0.95 V (*vs.* SCE) and then decreases. As shown in Fig. S8b, the influence of the deposition time of $[^{VI}UO_2^{2+} - Cupferron]$ complex was investigated using concentrations of UO_2^{2+} of 20.0 and 5.00 μg·L^{-1}. It was observed that the J_p of UO_2^{2+} increases linearly with the deposition time up to 180 s, and then more slowly up to 360 s. Therefore, the deposition potential of − 0.95V (*vs.* SCE) and the deposition time of 180 s were chosen for further study.

Analysis of performance

Under optimized conditions, UO_2^{2+} was detected by DPAdSV based on PBCB/GCE and compared with the previous bare GCE [4]. As shown in Fig. 5, the UO_2^{2+} peak current rises linearly with the increase of UO_2^{2+} concentration based on DPAdSV with the following calibration equation: $y = (90.7 \pm 0.87) + (27.1 \pm 0.76) \times$ ($R^2 = 0.997$) (Fig. 5a) and (I) $y = (104.2 \pm 1.33) + (5.03 \pm 0.15) \times$ ($R^2 = 0.996$) (II) $y = (190.8 \pm 0.75) + (0.935 \pm 0.025) \times$ ($R^2 = 0.999$) (Fig. 5b). The detection limit, calculated $3s_{bl}$/slope [50], was 0.067 μg·L^{-1} (Φ 1 mm) and 0.65μg·L^{-1}

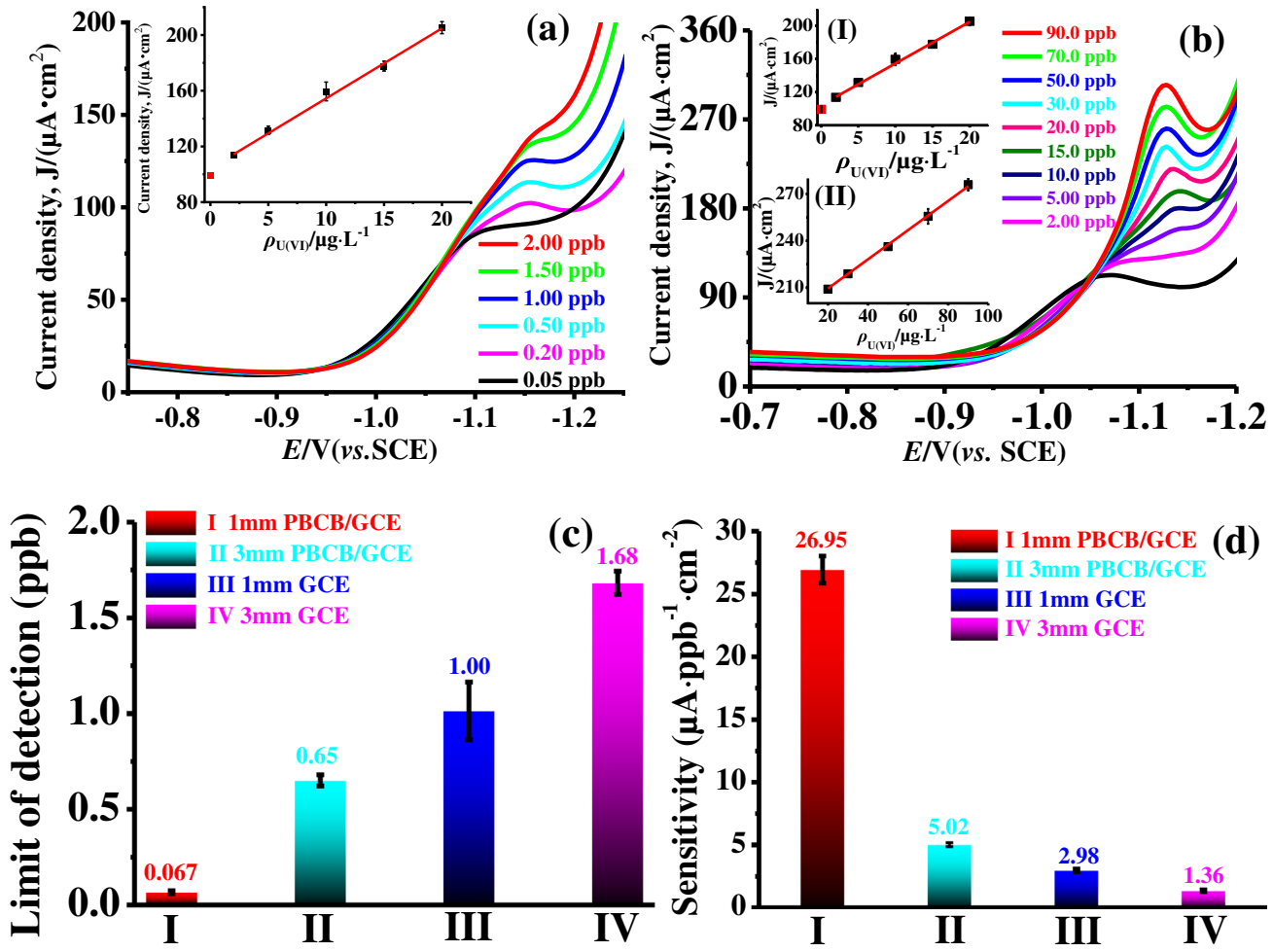

Fig. 5 The DPAdSV for different concentration of UO_2^{2+}. The inset shows plot of the peak current of the UO_2^{2+} concentration on **a** *Φ* 1 mm and **b** *Φ* 3 mm PBCB/GCE. **c** Corresponding limits of detection (LOD). **d** Comparison of sensitivity toward UO_2^{2+}

(*Φ* 3 mm) at − 0.113 V (*vs.* SCE), which were well below the concentration of 30.0 μg·L^{-1} by WHO guideline in drinking water [52]. Compared with previous work [4, 16], the PBCB/GCE obtained a satisfactory sensitivity for the lower concentration of UO_2^{2+} determination. The results illustrated that the PBCB/GCE demonstrated to be effective for the determination of UO_2^{2+} in sub-μgL^{-1} level by DPAdSV. Furthermore, the experimental evidence was performed as mentioned in the section of characterization of PBCB/GCE for the sensitivity improvement is original to PBCB polymer. Therefore, the polymer of PBCB was the major player in the sensitivity detection of UO_2^{2+}. Besides, the *Φ* 1 mm PBCB/GCE obtained higher sensitivity attributable to high current density [2, 47]. The *Φ* 1 mm PBCB/GCE obtained limit of detection rivals those of analytical instruments applied for UO_2^{2+} determination ICP-OES with 0.090 μg·$L^{-1}$and 0.57 μg·L^{-1} [22, 23], ICP-MS with 0.10 μg·L^{-1} [24], with fluorometric determination of UO_2^{2+} 6.53 μg·L^{-1}.

The PBCB/GCE was compared with other sensors for UO_2^{2+} analytical performance in Table 1. These results show that PBCB/GCE has the advantage in detection limit and quantification limit compared to all other sensors. Notably, Nassab et al. [32] reported that *N*-phenylanthranilic acid was used as a complexing agent for the determination of UO_2^{2+} by adsorptive cathodic stripping voltammetry on a mercury electrode, but the toxicity, handling, and disposal of mercury and its salts cannot be ignored. Without assistance of complexing, Nassab et al. [32] employed electropolymerized *N*-phenylanthranilic acid film electrode electrochemistry detection for UO_2^{2+}. However, the NPAA/GCE made use of metal ions with different redox potentials for selective detection of uranium. The PBCB/GCE has obtained good peaks for trace amounts of UO_2^{2+}, while other high-concentration metal ions have not obtained corresponding peaks.

Based on the above results, the PBCB/GCE high sensitivity determination of UO_2^{2+}possible mechanism model was proposed in Fig. 6. Compared with the conventional

Table 1 Comparison of analytical performance of PBCB/GCE with other sensors for detection of UO_2^{2+}

Number	Sensor	Method	Analysis time (s)	Linear range ($\mu g \cdot L^{-1}$)	Detection limit ($\mu g \cdot L^{-1}$)	Ref.
1	DNAzyme/AuNPs/BDT/Au	DPV[a]	–	0.0–1.19	–	[10]
2	Cyanopyridine-derived fluorescent	Florescence intensity	–	2.28–12566.4	0.004	[13]
3	GCOOH/GCE	SWAdSV[b]	1800	11.9–1190	–	[18]
4	GRA/PAA	SWV[c]	–	2.70–67.5	0.26	[20]
5	cat-1/Au–NP@CNTs	CV[d]	–	0.49–170	–	[14]
6	MUPA-SAM	DPAdSV[e]	1000	0.119–7.14	0.10	[19]
7	RuNPs/GCE	DPV[a]	–	45.2–352	1.95	[17]
8	Bismuth film electrode	SWAdSV[b]	600	10.0–300.0	0.30	[34]
9	NPAA/GCE	DPAdSV[e]	400	0.50–30.0	0.15	[15]
10	GCE	DPAdSV[e]	120	3.00–80.0	1.00	[4]
11	PNB/GCE	DPAdSV[e]	180	0.30 –90.0	0.19	[16]
12	PBCB/GCE	DPAdSV[e]	180	2.00–90.0 0.20–2.00	0.650 Φ 3 mm 0.067 Φ 1 mm	This work

[a]Square wave adsorptive stripping voltammetry

[b]Square wave voltammetry

[c]Cycle voltammetry

[d]Differential pulse adsorptive stripping voltammetry

[e]Differential pulse voltammetry

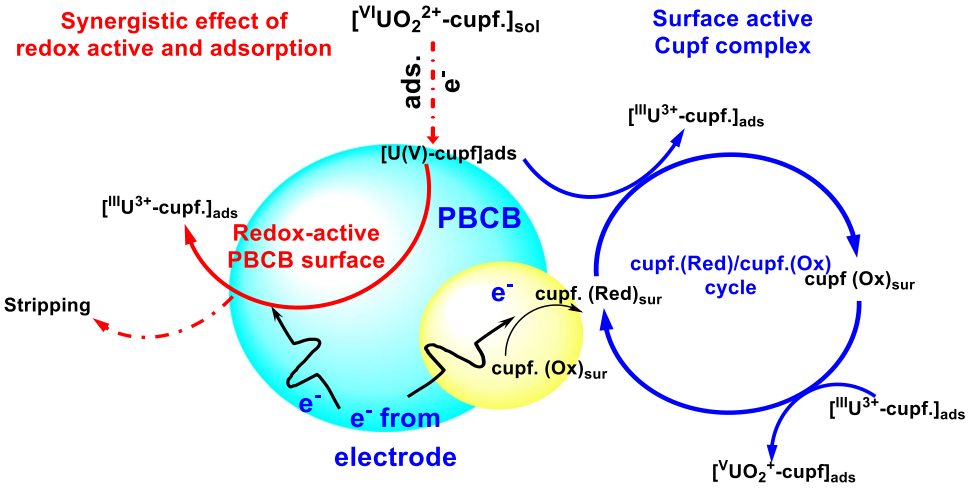

Fig. 6 High-sensitivity electrochemical determination of UO_2^{2+} based on PBCB/GCE

GCE, the PBCB/GCE exhibits excellent electrochemical performance and significantly improves the detection effect of UO_2^{2+}. The $[^{VI}UO_2^{2+} - Cupferron]_{ads}$ was obtained an electron, and it reduced to $[^{V}UO_2^{+} - Cupferron]_{ads}$ during potential deposition on the PBCB/GCE surface, and then the $[^{V}UO_2^{+} - Cupferron]_{ads}$ was obtained two electrons, and it reduced to $[^{III}U^{3+} - Cupferron]_{ads}$ at cathodic stripping process. In addition, the cupferron plays the double role of a complexing and oxidizing reagent [3, 4, 16, 35], leading to the parallel chemical re-oxidation of $[^{III}U^{3+} - Cupferron]_{ads}$ with $[^{V}UO_2^{+} - Cupferron]_{ads}$ and hence enhanced electrochemical signal of UO_2^{2+} (right side of Fig. 6). Meanwhile, the highly redox-active PBCB polymer was increasing the UO_2^{2+} stripping peak current (the left side of Fig. 6). In the whole detection of UO_2^{2+} process, the cupferron is not only a complexing agent but also an oxidizing agent. On the other hand, the PBCB may have acted as a reaction carrier [36, 37, 39, 43, 53], which oxidized $[^{III}U^{3+} - Cupferron]_{ads}$ to $[^{V}UO_2^{+} - Cupferron]_{ads}$. This improves the sensitivity of detecting UO_2^{2+}.

Repeatability, reproducibility, and interferences studies

To further demonstrate the application of PBCB/GCE, we investigated the repeatability and reproducibility of PBCB/

GCE in Fig. S9. A freshly prepared PBCB/GCE electrode was used for 10.0 μg·L^{-1} UO_2^{2+} nine parallel determinations, and the relative standard deviation (RSD) was 4.2% (n = 27) in Fig. S9a. Seven PBCB/GCE sensors, one fresh sensor every day, were applied for 10.0 μg·L^{-1} UO_2^{2+} parallel determination, and the RSD was 5.4 % (n = 21), in Fig. S9b. These results indicate the good repeatability and reproducibility of the sensor and its potential capacity for the detection of UO_2^{2+} in real environmental waters. Besides, the storage lifetime of the sensing was studied by storing the prepared electrode in 2~4 °C storage solutions (0.10 M pH 6.80 Na_2HPO_4/NaH_2PO_4 containing 0.20 M $NaNO_3$) for 10 days. The 70.06% of initial current was still retained after 10 days, indicating that the long-term stability of sensor remains challenging, in Fig. S10.

The presence of organic compounds (surfactants: nonionic Triton X-100, cationic CTAB, and anionic SDS) [4, 16, 33, 47] in natural environmental samples affected the determination of UO_2^{2+} complexes. As shown in Fig. 7, the analytical stripping signal of UO_2^{2+} decreased to 60% of its original value in the presence of 4.00 mg·L^{-1} of SDS, then the UO_2^{2+} peak increased and trended to level off at the higher concentration. In addition, 4.00 mg·L^{-1} Triton X-100 decreased the UO_2^{2+} signal by about 20%; however, peak sharply decreased at higher concentrations. Since environmental water samples usually contain 0.010–2.00 mg L^{-1} surfactant like Triton X-100 [54], there is almost no effect on the determination of UO_2^{2+}. The 4.00 mg L^{-1} CTAB surfactant causes interference effects, however, to a lesser extent. Furthermore, the influence of other metal ions on the stripping signal of

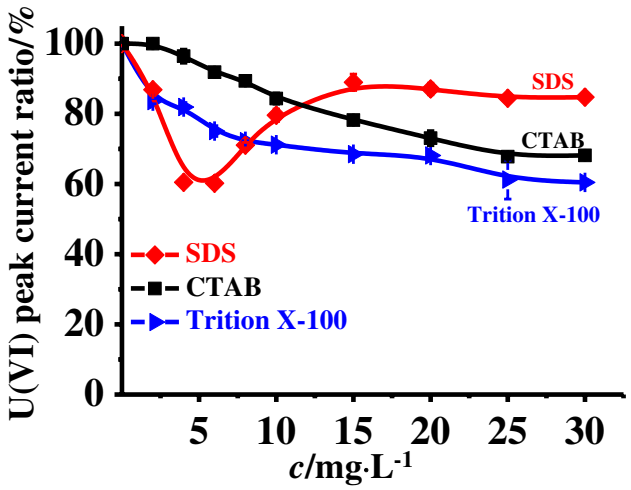

Fig. 7 Effect of surface-active substances (Triton X-100, SDS, CTAB) on 10.0 μg·L^{-1} UO_2^{2+} determination. Other conditions, as in Fig. 3b

Table 2 Maximum tolerance concentration of interfering species with 10.0 μg·L^{-1} UO_2^{2+} under optimum conditions

Metal ions	Tolerance concentration (μg·L^{-1})
Al^{3+}, Sr^{2+}, Sn^{2+}, Mg^{2+}, Pb^{2+}, Mn^{2+}, Ca^{2+}, Zn^{2+}, K^+	10,000
Co^{2+}, Fe^{3+}	5000
Cu^{2+}, Cr^{3+}	1000

10.0 μg·L^{-1} U(VI) is studied in Table 2. It was observed that the J_p of U(VI) was not influenced by a 1000-fold excess of Al^{3+}, Sr^{2+}, Sn^{2+}, Zn^{2+}, Ca^{2+}, Mg^{2+}, K^{2+} and Pb^{2+}; 500-fold excess of Fe^{3+}, Co^{2+}, and Cu^{2+}; 100-fold excess of Mn^{2+} and Cr^{2+}. Considering the Co^{2+}, Cu^{2+}, and Pb^{2+} are rarely present in natural water samples, the UO_2^{2+} may be detected directly in real environmental water samples.

Analytical applications

We carried out verification of the feasibility of the PBCB/GCE in practice use. Fig. S11 and Table S2 show good recovery rates of spiked amounts of UO_2^{2+} in the river water and tap water samples. However, the sea-water samples of recovery were further decreased to 79.0 % and 84.8 %, respectively. The origin of this impact factor was not clear but appears to be related to UO_2^{2+} speciation in sea water sample. Besides, the comparison test results of water samples, like tap water and river water samples, obtained from the DPAdSV were in accordance with those detected by ICP-MS, which confirmed the accuracy and precision of the proposed DPAdSV. Therefore, the PBCB/GCE seems to be a promising chemical sensor for the determination of uranyl in environmental water, like river water and tap water.

Conclusion

We proposed an electrochemistry sensor, electropolymerization BCB-modified GCE, to determine UO_2^{2+} in water samples by DPAdSV. In previous studies [2, 34, 47], factors such as scale of electrode, deposition potential, and times have been reported to enhance the detection of UO_2^{2+}. We uncovered several additional factors, like conductivity, electroactive area, and redox activity. The combination of adsorption stripping voltammetry (AdSV) and complexing agents further improves the analytical performance of PBCB/GCE, which is a practical and effective analytical method. In addition, the PBCB/

GCE was assessed for its analytical performance using tap water, river water, sea water, and interfering substances, such as SDS, Triton X-100, CTAB, and some metal ions. However, the PBCB/GCE was not suitable for the determination of UO_2^{2+} in sea waters containing high amounts of salt due to UO_2^{2+} speciation and other interfere ions in seawater. This work provided a novel perspective for the electroanalysis of UO_2^{2+} on the surface of PBCB/GCE, which could also be beneficial to developing sensitive electrochemical sensors for other heavy metal ions with redox active polymer.

Supplementary Information The online version contains supplementary material available at https://doi.org/10.1007/s00604-022-05485-1.

Funding This work is supported by the National Natural Science Foundation of China (Grant Nos. 22066004, 218660), Education Department of Jiangxi Province (Nos. GJJ170435), the Fundamental Science on Radioactive Geology and Exploration Technology Laboratory, East China University of Technology (Nos. RGET1907), and the State Key Laboratory of Nuclear Resources and Environment, East China University of Technology (Nos. 2020NRE29).

Declarations

Conflict of interest The authors declare no competing interests.

References

1. Farzin L, Shamsipur M, Sheibani S, Samandari L, Hatami Z (2019) A review on nanomaterial-based electrochemical, optical, photoacoustic and magnetoelastic methods for determination of uranyl cation. Microchim Acta 186:289. https://doi.org/10.1007/s00604-019-3426-5
2. Peled Y, Krent E, Tal N, Tobias H, Mandler D (2015) Electrochemical determination of low levels of uranyl by a vibrating gold microelectrode. Anal Chem 87:768–776. https://doi.org/10.1021/ac503719r
3. Zhang L, Wang CZ, Tang HB, Wang L, Liu YS, Zhao YL, Chai ZF, Shi WQ (2015) Rapid determination of uranium in water samples by adsorptive cathodic stripping voltammetry using a tin-bismuth alloy electrode. Electrochim Acta 174:925–932. https://doi.org/10.1016/j.electacta.2015.06.087
4. Zhiping Z, Yueming Z, Xizhen L, Fang X, Shujuan L, Jianguo M (2019) Sensitive detection of uranium in water samples using differential pulse adsorptive stripping voltammetry on glassy carbon electrode. J Radioanal Nucl Chem. https://doi.org/10.1007/s10967-019-06892-0
5. Şimşek S, Kaya S, Mine Şenol Z, İbrahim Ulusoy H, Katin KP, Özer A, Altunay N, Brahmia A (2022) Theoretical and experimental insights about the adsorption of uranyl ion on a new designed Vermiculite-Polymer composite. J Mol Liq 352:118727. https://doi.org/10.1016/j.molliq.2022.118727
6. Şimşek S, Şenol ZM, Ulusoy Hİ (2017) Synthesis and characterization of a composite polymeric material including chelating agent for adsorption of uranyl ions. J Hazard Mater 338:437–446. https://doi.org/10.1016/j.jhazmat.2017.05.059
7. Ulusoy Hİ, Şimşek S (2013) Removal of uranyl ions in aquatic mediums by using a new material: gallocyanine grafted hydrogel. J Hazard Mater 254–255:397–405. https://doi.org/10.1016/j.jhazmat.2013.04.004
8. Lee JH, Wang Z, Liu J, Lu Y (2008) Highly sensitive and selective colorimetric sensors for uranyl (UO_2^{2+}): development and comparison of labeled and label-free DNAzyme-Gold nanoparticle systems. J Am Chem Soc 130:14217–14226. https://doi.org/10.1021/ja803607z
9. Istok JD, Senko JM, Krumholz LR, Watson D, Bogle MA, Peacock A, Chang YJ, White DC (2004) In situ bioreduction of technetium and uranium in a nitrate-contaminated aquifer. Environ Sci Technol 38:468–475. https://doi.org/10.1021/es034639p
10. Chen L, Liu J, Cao C, Tang S, Lv C, Xiao X, Yang S, Liu L, Sun L, Zhu B, Li L (2021) Dual-signal amplification electrochemical sensing for the sensitive detection of uranyl ion based on gold nanoparticles and hybridization chain reaction-assisted synthesis of silver nanoclusters. Anal Chim Acta 1184:338986. https://doi.org/10.1016/j.aca.2021.338986
11. He W, Hua D (2019) Spectrographic sensors for uranyl detection in the environment. Talanta 201:317–329. https://doi.org/10.1016/j.talanta.2019.04.018
12. Zheng M, Yin Q, Wang D, Zhao Z, Hu Q, Wang H (2021) A fluorescent probe of uranyl for acid and high water system and imaging in living cells. Microchem J 167:106302. https://doi.org/10.1016/j.microc.2021.106302
13. Salem AR, El-Naggar AM, Mohamed EH, Amin MA, Attia MS (2022) A novel cyanopyridine derived fluorescent sensor for selective determination of uranyl ions in different water samples. J Radioanal Nucl Chem 331:187–196. https://doi.org/10.1007/s10967-021-08105-z
14. Muñoz J, Montes R, Bastos-Arrieta J, Guardingo M, Busqué F, Ruíz-Molina D, Palet C, García-Orellana J, Baeza M (2018) Carbon nanotube-based nanocomposite sensor tuned with a catechol as novel electrochemical recognition platform of uranyl ion in aqueous samples. Sens Actuators, B Chem 273:1807–1815. https://doi.org/10.1016/j.snb.2018.07.093
15. RashidiNassab H, Souri A, Javadian A, Amini MK (2015) A novel mercury-free stripping voltammetric sensor for uranium based on electropolymerized N-phenylanthranilic acid film electrode. Sens Actuators, B Chem 215:360–367. https://doi.org/10.1016/j.snb.2015.03.086
16. Zhou Z, Zhou Y, Liang X, Luo J, Liu S, Ma J (2022) Electrochemical sensor for uranium monitoring in natural water based on poly Nile blue modified glassy carbon electrode. J Solid State Electrochem. https://doi.org/10.1007/s10008-021-05102-w
17. Gupta R, Sundararajan M, Gamare JS (2017) Ruthenium nanoparticles mediated electrocatalytic reduction of UO_2^{2+} ions for Its rapid and sensitive detection in natural waters. Anal Chem 89:8156–8161. https://doi.org/10.1021/acs.analchem.7b01973
18. Ziolkowski R, Gorski L, Malinowska E (2017) Carboxylated graphene as a sensing material for electrochemical uranyl ion detection. Sensors and Actuators B-Chemical 238:540–547. https://doi.org/10.1016/j.snb.2016.07.119
19. Merli D, Protti S, Labò M, Pesavento M, Profumo A (2016) A ω-mercaptoundecylphosphonic acid chemically modified gold electrode for uranium determination in waters in presence of organic matter. Talanta 151:119–125. https://doi.org/10.1016/j.talanta.2016.01.032
20. Dimovasilis PA, Prodromidis MI (2011) An electrochemical sensor for trace uranium determination based on 6-O-palmitoyl-l-ascorbic acid-modified graphite electrodes. Sens Actuators, B Chem 156:689–694. https://doi.org/10.1016/j.snb.2011.02.019
21. Wu P, Hwang K, Lan T, Lu Y (2013) A DNAzyme-gold nanoparticle probe for uranyl ion in living cells. J Am Chem Soc 135:5254–5257. https://doi.org/10.1021/ja400150v

22. Akl ZF (2018) Sensitive quantification of uranium using cloud point extraction coupled with inductively coupled plasma-optical emission spectrometry. J Radioanal Nucl Chem 315:21–28. https://doi.org/10.1007/s10967-017-5642-y
23. Zari N, Hassan J, Tabar-Heydar K, Ahmadi SH (2020) Ion-association dispersive liquid–liquid microextraction of trace amount of gold in water samples and ore using Aliquat 336 prior to inductivity coupled plasma atomic emission spectrometry determination. J Ind Eng Chem 86:47–52. https://doi.org/10.1016/j.jiec.2017.01.038
24. Boomer DW, Powell MJ (1987) Determination of uranium in environmental samples using inductively coupled plasma mass spectrometry. Anal Chem 59:2810–2813. https://doi.org/10.1021/ac00150a019
25. Liu J, Brown Andrea K, Meng X, Cropek Donald M, Istok Jonathan D, Watson David B, Lu Y (2007) A catalytic beacon sensor for uranium with parts-per-trillion sensitivity and millionfold selectivity. Proc Natl Acad Sci 104:2056–2061. https://doi.org/10.1073/pnas.0607875104
26. Murthy RSS, Ryan DE (1983) Determination of arsenic, molybdenum, uranium, and vanadium in seawater by by neutron activation analysis after preconcentration by colloid flotation. Anal Chem 55:682–684. https://doi.org/10.1021/ac00255a023
27. Hosseini MA, Ahmadi M (2017) Miniature Neutron Source Reactors in medical research: achievements and challenges. J Radioanal Nucl Chem 314:1497–1504. https://doi.org/10.1007/s10967-017-5554-x
28. Wu X, Huang Q, Mao Y, Wang X, Wang Y, Hu Q, Wang H, Wang X (2019) Sensors for determination of uranium: a review. TrAC, Trends Anal Chem 118:89–111. https://doi.org/10.1016/j.trac.2019.04.026
29. Shrivastava A, Sharma J, Soni V (2013) Various electroanalytical methods for the determination of uranium in different matrices. Bulletin of Faculty of Pharmacy, Cairo University 51:113–129. https://doi.org/10.1016/j.bfopcu.2012.09.003
30. Wang J, Setiadji R (1992) Selective determination of trace uranium by stripping voltammetry following adsorptive accumulation of the uranium—cupferron complex. Anal Chim Acta 264:205–211. https://doi.org/10.1016/0003-2670(92)87007-8
31. Wang J, Wang J, Lu J, Olsen K (1994) Adsorptive stripping voltammetry of trace uranium: critical comparison of various chelating agents. Anal Chim Acta 292:91–97. https://doi.org/10.1016/0003-2670(94)00067-0
32. RashidiNassab H, Bakhshi M, Amini MK (2014) Adsorptive cathodic stripping voltammetric determination of uranium(VI) in presence of *N*-phenylanthranilic acid. Electroanalysis 26:1598–1605. https://doi.org/10.1002/elan.201400107
33. Tyszczuk-Rotko K, Jędruchniewicz K (2019) Ultrasensitive sensor for uranium monitoring in water ecosystems. J Electrochem Soc 166:B837–B844. https://doi.org/10.1149/2.1371910jes
34. Lin L, Thongngamdee S, Wang J, Lin Y, Sadik OA, Ly SY (2005) Adsorptive stripping voltammetric measurements of trace uranium at the bismuth film electrode. Anal Chim Acta 535:9–13. https://doi.org/10.1016/j.aca.2004.12.003
35. Tyszczuk-Rotko K, Domanska K, Czech B, Rotko M (2017) Development simple and sensitive voltammetric procedure for ultra-trace determination of U(VI). Talanta 165:474–481. https://doi.org/10.1016/j.talanta.2016.12.066
36. Ibanez JG, Rincón ME, Gutierrez-Granados S, Chahma Mh, Jaramillo-Quintero OA, Frontana-Uribe BA (2018) Conducting polymers in the fields of energy, environmental remediation, and chemical–chiral sensors. Chem Rev 118:4731–4816. https://doi.org/10.1021/acs.chemrev.7b00482
37. Nezakati T, Seifalian A, Tan A, Seifalian AM (2018) Conductive polymers: opportunities and challenges in biomedical applications. Chem Rev 118:6766–6843. https://doi.org/10.1021/acs.chemrev.6b00275
38. Pinaeva U, Dietz TC, Al Sheikhly M, Balanzat E, Castellino M, Wade TL, Clochard MC (2019) Bis[2-(methacryloyloxy)ethyl] phosphate radiografted into track-etched PVDF for uranium (VI) determination by means of cathodic stripping voltammetry. React Funct Polym 142:77–86. https://doi.org/10.1016/j.reactfunctpolym.2019.06.006
39. Heinze J, Frontana-Uribe BA, Ludwigs S (2010) Electrochemistry of conducting polymers—persistent models and new concepts. Chem Rev 110:4724–4771. https://doi.org/10.1021/cr900226k
40. Attar A, Emilia Ghica M, Amine A, Brett CMA (2014) Poly(neutral red) based hydrogen peroxide biosensor for chromium determination by inhibition measurements. J Hazard Mater 279:348–355. https://doi.org/10.1016/j.jhazmat.2014.07.019
41. Salinas G, Frontana-Uribe BA, Reculusa S, Garrigue P, Kuhn A (2018) Highly ordered macroporous poly-3,4-ortho-xylendioxythiophene electrodes as a sensitive analytical tool for heavy metal quantification. Anal Chem 90:11770–11774. https://doi.org/10.1021/acs.analchem.8b03779
42. Manisankar P, Vedhi C, Selvanathan G, Arumugam P (2008) Differential pulse stripping voltammetric determination of heavy metals simultaneously using new polymer modified glassy carbon electrodes. Microchim Acta 163:289–295. https://doi.org/10.1007/s00604-008-0013-6
43. Ding M, Zhou Y, Liang X, Zou H, Wang Z, Wang M, Ma J (2016) An electrochemical sensor based on graphene/poly(brilliant cresyl blue) nanocomposite for determination of epinephrine. J Electroanal Chem 763:25–31. https://doi.org/10.1016/j.jelechem.2015.12.040
44. Liang X, Zhou Y, Brett CMA (2022) Electropolymerisation of brilliant cresyl blue and neutral red on carbon-nanotube modified electrodes in binary and ternary deep eutectic solvents. J Electroanal Chem 919:116557. https://doi.org/10.1016/j.jelechem.2022.116557
45. Ricks AM, Gagliardi L, Duncan MA (2010) Infrared spectroscopy of extreme coordination: the carbonyls of U^+ and UO_2^+. J Am Chem Soc 132:15905–15907. https://doi.org/10.1021/ja1077365
46. Boncella JM (2008) Uranium gets a reaction. Nature 451:250. https://doi.org/10.1038/451250a
47. Gęca I, Ochab M, Korolczuk M (2020) Application of a solid lead microelectrode as a new voltammetric sensor for adsorptive stripping voltammetry of U(VI). Talanta 207:120309. https://doi.org/10.1016/j.talanta.2019.120309
48. Agarwal R, Sharma MK, Jayachandran K, Gamare JS, Noronha DM, Lohithakshan KV (2018) Poly(3,4-ethylenedioxythiophene)–poly(styrenesulfonate)-coated glassy-carbon electrode for simultaneous voltammetric determination of uranium and plutonium in fast-breeder-test-reactor fuel. Anal Chem 90:10187–10195. https://doi.org/10.1021/acs.analchem.8b00769
49. Aikens DA (1983) Electrochemical methods, fundamentals and applications. J Chem Educ. https://doi.org/10.1021/ed060pa25.1
50. Mocak J, Bond AM, Mitchell S, Scollary G (1997) A statistical overview of standard (IUPAC and ACS) and new procedures for determining the limits of detection and quantification: application to voltammetric and stripping techniques (Technical Report). Pure Appl Chem 69:297–328. https://doi.org/10.1351/pac199769020297

51. Barsan MM, Ghica ME, Brett CMA (2015) Electrochemical sensors and biosensors based on redox polymer/carbon nanotube modified electrodes: a review. Anal Chim Acta 881:1–23. https://doi.org/10.1016/j.aca.2015.02.059
52. Frisbie SH, Mitchell EJ, Sarkar B (2015) Urgent need to reevaluate the latest world health organization guidelines for toxic inorganic substances in drinking water. Environ Health 14:63–77. https://doi.org/10.1186/s12940-015-0050-7
53. Abney CW, Mayes RT, Saito T, Dai S (2017) Materials for the recovery of uranium from seawater. Chem Rev 117:13935–14013. https://doi.org/10.1021/acs.chemrev.7b00355
54. Grabarczyk M, Koper A (2011) How to determine uranium faster and cheaper by adsorptive stripping voltammetry in water samples containing surface active compounds. Electroanalysis 23:1442–1446. https://doi.org/10.1002/elan.201000657